electronics

MDPI

Article

Hybrid FSO/RF Communications in Space–Air–Ground Integrated Networks: A Reduced Overhead Link Selection Policy

Petros S. Bithas [1,*], Hector E. Nistazakis [2], Athanassios Katsis [3] and Liang Yang [4]

[1] Department of Digital Industry Technologies, National and Kapodistrian University of Athens (NKUA), 34400 Psahna, Greece
[2] Department of Physics, National and Kapodistrian University of Athens, 15784 Athens, Greece; enistaz@phys.uoa.gr
[3] Department of Social and Educational Policy, University of the Peloponnese, 20100 Korinthos, Greece; katsis@uop.gr
[4] College of Computer Science and Electronic Engineering, Hunan University, Changsha 410082, China; liangy@hnu.edu.cn
* Correspondence: pbithas@dind.uoa.gr

Abstract: Space–air–ground integrated network (SAGIN) is considered an enabler for sixth-generation (6G) networks. By integrating terrestrial and non-terrestrial (satellite, aerial) networks, SAGIN seems to be a quite promising solution to provide reliable connectivity everywhere and all the time. Its availability can be further enhanced if hybrid free space optical (FSO)/radio frequency (RF) links are adopted. In this paper, the performance of a hybrid FSO/RF communication system operating in SAGIN has been analytically evaluated. In the considered system, a high-altitude platform station (HAPS) is used to forward the satellite signal to the ground station. Moreover, the FSO channel model assumed takes into account the turbulence, pointing errors, and path losses, while for the RF links, a relatively new composite fading model has been considered. In this context, a new link selection scheme has been proposed that is designed to reduced the signaling overhead required for the switching operations between the RF and FSO links. The analytical framework that has been developed is based on the Markov chain theory. Capitalizing on this framework, the performance of the system has been investigated using the criteria of outage probability and the average number of link estimations. The numerical results presented reveal that the new selection scheme offers a good compromise between performance and complexity.

Keywords: composite fading; free space optical communications; hybrid FSO/RF communications; network selection; reduced signaling overhead; space–air–ground integrated networks

check for updates

Citation: Bithas, P.S.; Nistazakis, H.E.; Katsis, A.; Yang, L. Hybrid FSO/RF Communications in Integrated Space–Air–Ground Networks: A Low Complexity Channel Selection Policy. *Electronics* **2024**, *13*, 806. https://doi.org/10.3390/electronics13040806

Academic Editor: Christos J. Bouras

Received: 8 January 2024
Revised: 2 February 2024
Accepted: 15 February 2024
Published: 19 February 2024

1. Introduction

In recent years, the concept of space–air–ground integrated network (SAGIN), which integrates satellite, aerial, and terrestrial communications, has emerged as a noteworthy architectural paradigm [1]. This integrated approach has received significant research attention in an evolving and compelling area of study such as the sixth-generation (6G) communication network [2]. SAGIN aims to address the connectivity challenges that arise in remote and hard-to-reach areas by offering a cost-effective and high-capacity solution. Therefore, this type of network seems to be the only path towards realizing the Internet of remote things. However, despite the undoubted benefits of these networks, they also come with certain disadvantages, including unbalanced distribution of resources [3], channel impairments [4], complexity and integration challenges [5], and security concerns [2]. SAGIN can overcome some of the limitations associated with traditional communication methods by incorporating free space optical (FSO) systems. In general, combining FSO and radio frequency (RF) communications in hybrid systems is a promising approach, addressing limitations and enhancing performance for improved throughput, reliability, and energy efficiency [6].

As far as FSO-assisted SAGINs are concerned, these types of systems will lead to improved performance, reliability, and adaptability in diverse operational scenarios, since they will offer increased bandwidth availability, low latency, increased security, and immunity to electromagnetic interference [7]. However, FSO communications are also prone to various environmental and channel attenuation effects, e.g., atmospheric turbulence, that result in severe degradation of the performance, e.g., [8,9]. An alternative approach to mitigating the impact of atmospheric turbulence involves integrating RF links alongside the FSO ones to exploit their complementary attributes. This hybrid RF/FSO communication strategy allows for the advantages of both RF and FSO technologies, as a result effectively minimizing the detrimental effects associated with adverse weather conditions [10]. The performance of these systems can be further enhanced if unmanned aerial vehicles (UAVs) or high-altitude platform stations (HAPS) are used as relays [11,12]. The cooperation of HAPS and low Earth orbit (LEO) satellites is expected to guarantee higher capacity with lower propagation delay.

1.1. Relevant Works

In the past few years, there have been numerous contributions within the realm of integrated networks that combine FSO and RF technologies with satellite and aerial components, e.g., [13–21]. In [13], an analytical expression for the outage probability (OP) in a SAGIN has been presented, taking into account the impact of pointing errors in the satellite–aerial segment. In [14], based on the selective decode-and-forward (DF) protocol, the ergodic capacity of a multiuser downlink SAGIN has been analytically studied. In [15], the performance and the coverage of a communication system employing FSO-RF transmission is enhanced by employing a dual-hop configuration with a reconfigurable intelligent surface (RIS). In [16], a low-altitude platform (LAP)-aided dual-hop relaying system with non-orthogonal multiple access (NOMA) and FSO/RF communication has been explored. In this framework, an analysis has been provided that includes outage probability and asymptotic considerations, revealing that LAP altitude and FSO channel parameters significantly impact system performance. In [17], the assessment of a dual-hop hybrid FSO/RF SAGIN has been analytically investigated using the criteria of OP and bit error probability. In [18] an HAPS-selection scheme was introduced in a cooperative SAGIN communication scenario. This scheme was based on a signal-to-noise ratio (SNR) criterion, while the OP analysis that was presented also took into account various impairment effects, including atmospheric turbulence and pointing errors.

In [19], the utilization of a LEO satellite was explored in order to enhance the performance of two mixed FSO/RF HAPS-assisted communication systems. Moreover, Ref. [20] focuses on a hybrid FSO/RF and SAGIN, in which the OP and the average symbol error probability were investigated, also taking into account various propagation phenomena such as turbulence and weather effects. Finally, in [21], the performance of hybrid FSO/RF relay systems in a satellite terrestrial integrated network was investigated, and the effect of weather conditions was also taken into consideration. In that study, three different schemes were designed on HAPS, while reconfigurable intelligent surface (RIS)-assisted UAVs were also considered. It is noted that in most of the aforementioned studies, valuable insights were provided based on the asymptotic expressions that were also provided. Moreover, another parameter that is very important for the performance of hybrid RF/FSO SAGIN is signaling overhead. In particular, for the various network operations that frequently take place in these systems, e.g., handover and link switching, signaling exchanges between the network nodes should be made. However, this signaling is responsible for latency increase and effective capacity reduction. Therefore, algorithms that efficiently achieve a trade-off between signaling overhead and system performance should be proposed [22,23].

1.2. Contributions

Motivated by the aforementioned, in this paper, we introduce a lower signaling overhead channel selection scheme in hybrid FSO/RF SAGIN, which actually represents a low-complexity network selection technique. More specifically, the contributions of this paper are summarized as follows:

- A new channel selection scheme has been proposed and used in a hybrid FSO/RF SAGIN dual-hop communication scenario. The new scheme is designed to offer reduced overhead signaling with satisfactory performance.
- For the new scheme, the Markov chain theory has been employed to derive exact analytical expressions for the statistics of the end-to-end output SNR. The analysis presented also takes into account the impact of atmospheric turbulence and pointing errors (for the FSO link) as well as multipath fading and shadowing (for the RF link).
- In the high SNR regime, simpler asymptotic closed-form expressions are also provided, which have been used to elaborate on the physical insights of the considered scenarios.
- The analytical results derived are used to study the OP of the proposed scheme, while the signaling overhead has also been quantified using the criteria of average number of links estimation (NLE) and switching probability (SP).
- The numerical evaluated results presented reveal the reduction in the computational complexity (in terms of signaling overhead), which results in important energy savings without significantly affecting the system's performance.

The remainder of this paper is organized as follows. In Section 2, the system and channel models, as well as the mode of operation of the network selection technique proposed, are presented. In Section 3, a Markov chain-based analytical framework is presented which is used to investigate the end-to-end OP. In Section 4, various numerically evaluated results are presented and discussed, while in Section 5, the conclusions can be found.

2. System and Channel Models

In this section, the system and channel models under consideration are described, while the new link selection policy is also presented.

2.1. System Model

We consider a dual-hop SAGIN where the LEO satellite (S) communicates with the ground station (G) with the aid of an HAPS (H), as is shown in Figure 1. The direct S-G link is assumed to be blocked due to severe shadowing and atmospheric attenuation phenomena. In the proposed system, it is assumed that communication transmissions are performed in two orthogonal phases. In the first phase of communication, S transmits the signal to H using an FSO link. In that case, the received SNR at the HAPS is given by ([17] [Equation (7)]) (Without losing the generality, it is assumed that at the received SNR, subscript 1 denotes FSO links and subscript 2 denotes RF links)

$$\gamma_1 = \frac{\left(\eta P_f G_{Tf} G_{Rf} I\right)^b}{F^b \sigma_f^2}, \tag{1}$$

where η denotes the optical-to-electrical conversion coefficient, P_f denotes the transmit power of the FSO communication system, G_{Tf}, G_{Rf} are the transmit and receive telescope gains, respectively, I denotes the random fluctuations of the received amplitude, $F = (4\pi d_k/\lambda_f)$, where λ_f is the wavelength of the FSO communications, and d_k denotes the transmission distance between the FSO transmitter and FSO receiver (with $k \in s, h$), as is also shown in Figure 1. Moreover, $b = 1$ and $b = 2$ for heterodyne and direct detection schemes, respectively, while σ_f^2 denotes the noise variance of the additive white Gaussian noise (AWGN).

The H acts as a relay and implements DF protocol. Therefore, in the second phase of communications, if H has correctly decoded the signal received from the satellite, it forwards it to the G using hybrid RF/FSO communications. The received FSO signal at the G is characterized by an instantaneous SNR of the form presented in (1).

As far as the RF communication links are concerned, the instantaneous received SNR per symbol at the G is given by ([17] [Equation (12)])

$$\gamma_2 = \bar{\gamma}_2 |h_r|^2, \tag{2}$$

where $\bar{\gamma}_2$ is defined as

$$\bar{\gamma}_2 = \frac{P_t}{N_0}\left(\frac{G_{Tr} G_{Rr} \lambda_r^2}{16\pi^2 d_h^v}\right). \tag{3}$$

In (3), G_{Tr} and G_{Rr} denote the transmit and receive antenna gains for the RF systems, respectively, λ_r is the RF wavelength, and d_h denotes the H-G distance. Moreover, $|h_r|$ denotes the normalized magnitude of the channel fading coefficient; $|\cdot|$ denotes absolute value.

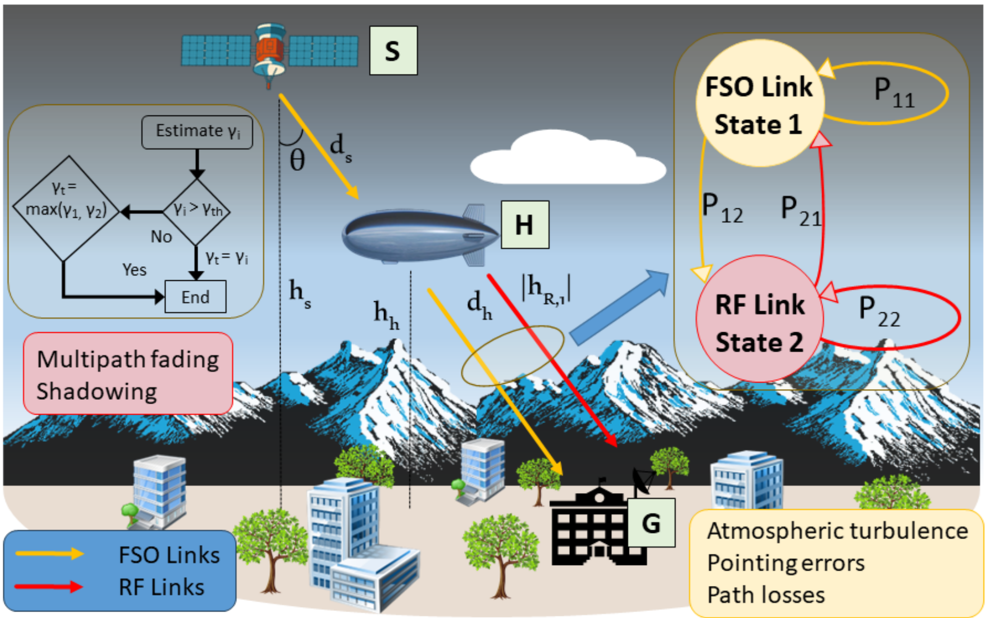

Figure 1. HAPS-assisted hybrid FSO/RF satellite communications system: Proposed mode of operation that is based on a two-state Markov chain.

Link Selection Policy

At the G, a new link (or network) selection policy is adopted which offers reduced overhead in terms of channel monitoring operations and signaling exchanges. The proposed mode of operation of this policy is also depicted in Figure 1. In particular, two states are defined with regards to the communication system that has been employed, namely, the FSO (State 1) and the RF (State 2). State selection is performed on T_p time-based period. More specifically, in each T_p the received SNR at G of the previously selected state is examined if it exceeds a predefined switching threshold γ_{th}. If this is the case, the system's algorithm selects to remain with that link; otherwise, it switches to the link (after examining both RF and FSO ones) that provides the highest SNR value at the G. Based on this approach, it is not necessary to continuously monitor the received SNR from both links in order to select the maximum, since in many cases the received SNR from one link will exceed γ_{th}. As a result, a reduced number of links estimations are expected to be performed.

Based on the above definitions, the end-to-end received instantaneous SNR at the G is given by

$$\gamma_o = \min\{\gamma_1, \gamma_t\} \tag{4}$$

where γ_t denotes the instantaneous received SNR at the G for the H-G link as a result of the mode of operation of the proposed policy. Next, the channel models assumed for both communication links are presented.

2.2. Channel Model

For the FSO links, the joined impacts of atmospheric turbulence-induced fading (modeled using the gamma–gamma distribution [24]), pointing errors (modeled using the Rayleigh distribution [25]), and path loss (based on the Beers–Lampert law [26]) have been taken into account. In that case, it can be proved that the cumulative distribution function (CDF) of the received SNR is given by ([17] [Equation (18)])

$$F_{\gamma_1}(\gamma) = \mathcal{A} G_{b+1,3b+1}^{3b,1}\left(\frac{D^b \gamma}{b^{2b}\bar{\gamma}_1^f}\middle|_{\Delta_{b,\zeta^2},\Delta_{b,\alpha},\Delta_{b,\beta},0}^{1,\Delta_{b,\zeta^2+1}}\right), \tag{5}$$

where $D = \alpha\beta\kappa$, $\mathcal{A} = \frac{\zeta^2 b^{\alpha+\beta-2}}{(2\pi)^{b-1}\Gamma(\alpha)\Gamma(\beta))}$, $\Delta_{x,y} = \frac{y}{x}, \frac{y+1}{x}, \frac{y+x-1}{x}$, while $\bar{\gamma}_1^f$ denotes the average received SNR defined as

$$\bar{\gamma}_1 = \frac{\eta P_f G_{Tf} G_{Rf} \kappa I_p^f A_0}{F_f^b \sigma_f^2}, \tag{6}$$

with $\kappa = \frac{\zeta^2}{\zeta^2+1}$. Moreover, I_p^f denotes the path loss attenuation, A_0 is the fraction of total power collected at the receiver aperture, and F_f is the free space loss defined as $F_f = \frac{4\pi d_k}{\lambda_f}$. Moreover, ζ denotes the pointing error parameter coefficient, while α and β are large- and small-scale turbulence parameters, respectively, related to the scattering environment, whose expressions are analytically provided below. Finally, $G_{p,q}^{m,n}[\cdot|\cdot]$ denotes the Meijer's G-function ([27] [Equation (9.301)]), and $\Gamma(\cdot)$ the gamma function ([27] [Equation (8.310/1)]). The corresponding PDF expression is given by ([17] [Equation (17)])

$$f_{\gamma_1}(\gamma) = \frac{\mathcal{B}}{\gamma} G_{1,3}^{3,0}\left(D\left(\frac{\gamma}{\bar{\gamma}_1^f}\right)^{1/b}\middle|_{\zeta^2,\alpha,\beta}^{\zeta^2+1}\right), \tag{7}$$

where $\mathcal{B} = \frac{\zeta^2}{b\Gamma(\alpha)\Gamma(\beta)}$. As far as the large- and small-scale turbulence parameters are concerned, they are, respectively, defined as ([24] [Equations (7a) and (7b)])

$$\alpha = \left\{5.95(h_k - h_\ell)^2 \sec(\theta)^2 \left(\frac{2W_0}{r}\right)^{5/3}\left(\frac{\Delta_{pe}}{W}\right)^2 + \left[\exp\left(\frac{0.49\sigma^2}{(1+0.56\sigma^{12/5})^{7/6}}\right) - 1\right]\right\}^{-1}, \tag{8}$$

$$\beta = \left[\exp\left(\frac{0.51\sigma^2}{(1+0.69\sigma^{12/5})^{5/6}}\right) - 1\right]^{-1}, \tag{9}$$

where the pair k, ℓ takes values s, h when S-H link is considered and h, p, when H-G link is considered. Next, the various parameters included in (8) and (9) will be analytically discussed. More specifically, in (8), σ^2 denotes the Rytov variance and is given by

$$\sigma^2 = 2.25 k_1^{7/6}(h_k - h_\ell)^{5/6}\sec(\theta)^{11/6} \times \int_{h_\ell}^{h_k} C_n^2(h)\left(1 - \frac{h-h_\ell}{h_k - h_\ell}\right)^{5/6}\left(\frac{h-h_\ell}{h_k-h_\ell}\right)^{5/6} dh. \tag{10}$$

Moreover, $C_n^2(h)$ denotes the refractive index structure parameter, which is defined as [28]

$$\begin{aligned} C_n^2(h) = 0.00594\left(\frac{w}{27}\right)^2\left(10^{-5}h\right)^{10}\exp\left(-\frac{h}{1000}\right) \\ + 2.7\cdot 10^{-16}\exp\left(-\frac{h}{1500}\right) + C_n^2(0)\exp\left(-\frac{h}{100}\right), \end{aligned} \quad (11)$$

where $C_n^2(0) = 1.7\times 10^{-14}m^{-2/3}$ and w denotes the wind velocity. Moreover, in (8), W_0 denotes the beam size at the transmitter, while the corresponding parameter at the receiver is given by $W = W_0\sqrt{\Theta^2 + \Lambda^2}$, where $\Theta = 1 - \frac{d_k}{F_0}$ and $\Lambda = \frac{2d_k}{k_1 W_0^2}$. Furthermore, F_0 denotes the phase front radius of the curvature of the beam at the transmitter and $d_k = \frac{h_k}{\cos(\theta)}$. Additionally, the Fried parameter r is given by

$$r = \left[0.42\sec(\theta)k_1^2\int_{h_\ell}^{h_k} C_n^2(h)dh\right]^{-3/5}, \quad (12)$$

while $\Delta_{pe} = \frac{\sigma_{pe}^2}{d_k}$ denotes the beam-wander-induced pointing errors, with the beam-wander-induced pointing error variance given by

$$\begin{aligned} \sigma_{pe}^2 = 0.54(h_k - h_\ell)^2\sec(\theta)^2\left(\frac{\lambda_f}{2W_0}\right)^2 \\ \times\left(\frac{2W_0}{r}\right)^{5/3}\left[1 - \left(\frac{C_r^2W_0^2/r^2}{1 + C_r^2W_0^2/r^2}\right)^{1/6}\right], \end{aligned} \quad (13)$$

with $C_r = 2\pi$ being the scaling constant.

For the RF links, the PDF of the instantaneous received SNR at the G can be expressed as ([29] [Equation (7)])

$$f_{\gamma_2}(\gamma) = \gamma^{-1}\mathcal{S}_1 G_{2,2}^{2,2}\left(\frac{m_1 m_2\gamma}{\bar{\gamma}_2}\middle|\begin{matrix}1-\alpha_2, 1-\alpha_1\\ m_1, m_2\end{matrix}\right), \quad (14)$$

where $\mathcal{S}_1 = \frac{1}{\Gamma(m_1)\Gamma(m_2)\Gamma(\alpha_1)\Gamma(\alpha_2)}$. It is noted that (14) is an experimentally verified composite fading model that accurately describes both small-scale and large-scale fading effects in UAV-to-ground communication scenarios. In particular, coefficients m_1, m_2 describe the severity of the small-scale fading effects, i.e., as m_1, m_2 increase, line-of-sight conditions are approximated. On the other hand, coefficients α_1, α_2 are related to the severity of the shadowing (large-scale fading) effects, i.e., lower values of α_1, α_2 result in lighter shadowing conditions. The corresponding CDF expression is given by ([29] [Equation (12)])

$$F_{\gamma_2}(\gamma) = \mathcal{S}_1 G_{3,3}^{2,3}\left(\frac{m_1 m_2\gamma}{\bar{\gamma}_2}\middle|\begin{matrix}1-\alpha_2, 1-\alpha_1, 1\\ m_1, m_2, 0\end{matrix}\right). \quad (15)$$

3. Markov Chain-Based Statistical Analysis

Based on the mode of operation that was presented in the previous section, in the proposed selection policy, a two-state ergodic and regular Markov chain is defined, whose state 1 corresponds to the event that transmission is performed using the FSO link and whose state 2 corresponds to the event that transmission is performed with the aid of RF link (see Figure 1). This Markov chain is characterized by a unique vector of stationary probabilities given by $\boldsymbol{\pi} = [\pi_1, \pi_2]$. Based on the fact that the previously mentioned events are mutually exclusive, the CDF of the output SNR at the G using the proposed scheme, γ_t, can be expressed as ([30] [Equation (3)])

$$F_{\gamma_t}(\gamma) = \begin{cases} \sum_{i=1}^{2} \pi_i \{ \Pr[\gamma_{\text{th}} \leq \gamma_i \leq \gamma] + \Pr[\gamma_i < \gamma_{\text{th}}] \\ \qquad \times \Pr[\gamma_2 \leq \gamma] \}, \gamma \geq \gamma_{\text{th}} \\ \Pr[\max\{\gamma_1, \gamma_2\} \leq \gamma], \quad \gamma < \gamma_{\text{th}}, \end{cases} \tag{16}$$

where γ_i, with $i \in \{1,2\}$ denotes the instantaneous received SNR from link i. Applying the definition of the CDF, i.e., $F_{\gamma_i}(x) = \Pr[\gamma_i < x]$, on the generic expression presented in (16), the following result is obtained

$$F_{\gamma_t}(\gamma) = \begin{cases} \sum_{i=1}^{2} \pi_i \{ F_{\gamma_i}(\gamma) - F_{\gamma_i}(\gamma_{\text{th}}) \\ \quad + F_{\gamma_i}(\gamma_{\text{th}}) F_{\gamma_{\bar{i}}}(\gamma) \}, \ \gamma \geq \gamma_{\text{th}} \\ F_{\gamma_1}(\gamma) F_{\gamma_2}(\gamma), \quad \gamma < \gamma_{\text{th}}, \end{cases} \tag{17}$$

where $F_{\gamma_1}(\cdot), F_{\gamma_2}(\cdot)$ are given by (5) and (15), respectively, while $\bar{i} = 3 - i$. Moreover, by differentiating (17) with respect to γ, the following expression for the PDF of γ_t can be obtained

$$f_{\gamma_t}(\gamma) = \begin{cases} \sum_{i=1}^{2} \pi_i \{ f_{\gamma_i}(\gamma) + F_{\gamma_i}(\gamma_{\text{th}}) f_{\gamma_{\bar{i}}}(\gamma) \}, \gamma \geq \gamma_{\text{th}} \\ \sum_{i=1}^{2} f_{\gamma_i}(\gamma) F_{\gamma_{\bar{i}}}(\gamma), \quad \gamma < \gamma_{\text{th}}, \end{cases} \tag{18}$$

where $f_{\gamma_1}(\cdot)$ and $f_{\gamma_2}(\cdot)$ are given by (7) and (14), respectively.

Due to the ergodicity of the Markov chain of our system, the aforementioned stationary probabilities can be evaluated using $\boldsymbol{\pi} = \boldsymbol{\pi} \cdot \mathbf{P}$ in conjunction with $\sum_{i=1}^{2} \pi = 1$, where $\mathbf{P}$ denotes the transition matrix given by Section 7.3 in [31]

$$\mathbf{P} = \begin{pmatrix} P_{11} & P_{12} \\ P_{21} & P_{22} \end{pmatrix}. \tag{19}$$

Exploiting (19), the stationarity probabilities can be obtained as follows

$$\begin{aligned} \pi_1 &= \frac{P_{21}}{P_{12} + P_{21}} \\ \pi_2 &= \frac{P_{12}}{P_{12} + P_{21}} \end{aligned} \tag{20}$$

In (19), the transition probabilities of the corresponding Markov chain can be evaluated based on the following observations. The probability of remaining at the same State i is equal to the sum of the probability of the received SNR from State i, i.e., γ_i, being larger than γ_{th} and the probability γ_i being lower than γ_{th} and simultaneously being larger than the received SNR from the other state, i.e., γ_j. The same approach is also followed for obtaining the probability of switching states from i to h or vice versa. From the mathematical point of view, this statement can analytically be expressed as

$$P_{i,j} = \begin{cases} \Pr[\gamma_i \geq \gamma_{\text{th}}] + \Pr[\gamma_i < \gamma_{\text{th}}, \gamma_i \geq \gamma_j], \ i = j \\ \Pr[\gamma_i < \gamma_{\text{th}}, \gamma_j \geq \gamma_i], \quad i \neq j. \end{cases} \tag{21}$$

In (21), it is obvious that

$$\Pr[\gamma_i \geq \gamma_{\text{th}}] = 1 - F_{\gamma_i}(\gamma_{\text{th}}). \tag{22}$$

Moreover, based on the fact that the random variables that model the instantaneous received SNR, i.e., γ_i and γ_2, are independent, and using basic probability theory, the second probability appearing in (21) can be evaluated as follows

$$\begin{aligned}\Pr[\gamma_i < \gamma_{\rm th}, \gamma_i \geq \gamma_j] &= \int_0^{\gamma_{\rm th}} \int_0^{x} f_{\gamma_j}(y) f_{\gamma_i}(x) dy dx \\ &= \int_0^{\gamma_{\rm th}} F_{\gamma_j}(x) f_{\gamma_i}(x) dx.\end{aligned} \tag{23}$$

Furthermore, when $i \neq j, P_{i,j} = 1 - P_{i,i}$. All these transition probabilities can be efficiently evaluated by substituting the corresponding PDF and CDF expressions in (22), (23) and employing the Gauss–Laguerre quadrature method [32].

4. Performance Analysis

In this section, analytical expressions for important performance metrics of the scheme under consideration will be provided. More specifically, its performance will be evaluated using the criteria of OP, average NLE, and SP.

4.1. Outage Probability

The OP is defined as the probability that the end-to-end instantaneous SNR falls below a predefined threshold γ_T and can be mathematically expressed as

$$P_{\rm out} = \Pr[\gamma_o \leq \gamma_T] = F_{\gamma_o}(\gamma_T). \tag{24}$$

Since a DF relay protocol has been assumed, the CDF of the received SNR γ_o can be expressed as

$$F_{\gamma_o}(\gamma_T) = F_{\gamma_1}(\gamma_T) + F_{\gamma_t}(\gamma_T) - F_{\gamma_1}(\gamma_T) F_{\gamma_t}(\gamma_T), \tag{25}$$

where $F_{\gamma_1}(\gamma_T)$ is given by (5) and $F_{\gamma_t}(\gamma_T)$ is given by (17).

High SNR Analysis

In the high SNR regime, asymptotic and easy-to-evaluate expressions can be derived that can be used to provide insights into the behavior of a system as the SNR increases without needing to rely on detailed numerical evaluations. This helps researchers gain a deeper understanding of how the system behaves in the high SNR limit. In the high SNR regime, i.e., $\bar{\gamma}_1, \bar{\gamma}_2 \to \infty$, simpler expressions for (5) and (15) can be obtained. More specifically, using ([33] [Equation (07.34.06.0006.01)]) in (5) and after some mathematical simplifications, the following asymptotic closed-form expression is obtained for the CDF of γ_1

$$F_{\gamma_1}(\gamma) \approx \sum_{k=1}^{3b} \frac{\mathcal{A}_i \prod\limits_{\substack{j=1 \\ j\neq k}}^{3b} \Gamma(\mathcal{B}_j - \mathcal{B}_k) \Gamma(1 - \mathcal{D}_1 + \mathcal{B}_k)}{\prod\limits_{j=2}^{b+1} \Gamma(\mathcal{D}_j - \mathcal{B}_k) \Gamma(1 - \mathcal{B}_{3b+1} + \mathcal{B}_k)} \left(\frac{D_i^b \gamma}{b^{2b} \bar{\gamma}_i^f} \right)^{\mathcal{B}_k}, \tag{26}$$

where $\mathcal{D}_1 = 1, \mathcal{D}_2 = \Delta_{b,\zeta_i^2+1}, \mathcal{B}_1 = \Delta_{b,\zeta_i^2}, \mathcal{B}_2 = \Delta_{b,\alpha_i}, \mathcal{B}_3 = \Delta_{b,\beta_i}, \mathcal{B}_4 = 0$. From the above expression, it becomes evident that the diversity gain (G_d) for FSO links, given by $(\bar{\gamma}_i^f)^{-G_d}$ as $\bar{\gamma}_i^f \to \infty$, depends on the small- and large-scale turbulence parameters as well as the pointing error coefficient.

As far as the RF link is concerned, by following the same procedure for (15), the corresponding expression is given by

$$F_{\gamma_2}(\gamma) \approx \mathcal{S}_1 \sum_{i=1}^{2} \frac{\Gamma(m_{3-i} - m_i)\Gamma(m_i + \alpha_2)\Gamma(m_i + \alpha_1)\Gamma(m_i)}{\Gamma(m_i + 1)} \left(\frac{m_1 m_2 \gamma}{\bar{\gamma}_2} \right)^{m_i}. \tag{27}$$

Following the same approach used for the FSO link, it can be shown that diversity gain for the RF link depends only on the small-scale fading parameters.

4.2. Overhead Estimation

In order to quantify the overhead signaling required for the operation of the scheme under consideration, two performance metrics will be adopted, namely, the average NLE and the SP.

4.2.1. Average Link Estimation

The overhead and signaling required for allowing the proposed scheme to properly function are linearly related to the average NLE $N = P_1 + 2 \cdot P_2$. This metric can be evaluated as the probability that exactly one path is examined which is equal to $P_1 = \pi_1 \Pr[\gamma_1 \geq \gamma_{\text{th}}] + \pi_2 \Pr[\gamma_2 \geq \gamma_{\text{th}}]$ plus the probability that both paths are examined $P_2 = \pi_1 \Pr[\gamma_1 < \gamma_{\text{th}}] + \pi_2 \Pr[\gamma_2 < \gamma_{\text{th}}]$. Substituting the corresponding CDF expressions in these definitions yields the following expression

$$N = \pi_1 (1 + F_{\gamma_1}(\gamma_{\text{th}})) + \pi_2 (1 + F_{\gamma_2}(\gamma_{\text{th}})). \tag{28}$$

From the above equation, it can be concluded that the NLE increases as γ_{th} increases until it reaches its maximum value which is 2, i.e., both links are always examined before selecting the one that offers the maximum SNR.

4.2.2. Switching Probability

Switching between the two links results in increased signaling and also consumes more power. Therefore, SP is one more metric which is related to the overhead signaling of the proposed scheme. This (switching) probability can be evaluated using the complementary ones, i.e., $P_{1,1}$ or $P_{2,2}$, which are conditioned to the corresponding stationary distributions π_1 and π_2, which results in the following closed-form expression

$$S_p = \pi_1 (1 - P_{11}) + \pi_2 (1 - P_{22}). \tag{29}$$

5. Numerical Results and Discussion

In this section, based on the previously presented theoretical analysis, numerical evaluated results are presented and discussed. If not otherwise stated, the values of the parameters considered in these results can be found in Table 1 and are mainly based on previous relevant studies, e.g., [20]. Moreover, for comparison purposes, we have also investigated the performance of a scheme in which in the second phase of communication, the link with the highest SNR, between the RF and the FSO, is always selected. This selection policy is also adopted in [18]. The numerical evaluation of the analytical expressions has been performed using the Mathematica software package. In particular, Mathematica supports all necessary functions for obtaining these results, such as the `NIntegrate[]` (for numerical integration) and `MeijerG[]` (for implementation of the Meijer's G function).

Table 1. Communication parameter definitions and simulation values.

Parameter	Definition	Value
λ_f	FSO wavelength	1550 nm
h_s	Satellite height	620 km
h_h	HAPS height	20 km
h_p	Ground station height	10 m
G_{Tf}	Transmit telescope gain	5 dB
P_f	FSO transmit power	5 dBm
G_{Rf}	Receive telescope gain	10 dB

Table 1. *Cont.*

Parameter	Definition	Value
σ_f^2	Variance of the AWGN noise	$4.435 \cdot 10^{-28}$
η	Optical to electrical conversion coefficient	0.8
ζ_i	Pointing error coefficient	13.07
θ	Zenith angle	65°
w	Wind velocity	4 Lm/s
W_0	Beam radius at the transmitter	2 cm
F_0	Phase front radius of curvature of the beam	∞
m_1, m_2	Small-scale fading shaping parameters	2.5, 2.8
α_1, α_2	Shadowing shaping parameters	1.2, 1.4
v	Path loss factor	2.1
P_t	Transmit power for RF communications	20 dBm
N_0	Noise power	−97.8 dBm
G_{T_r}	RF transmit antenna gain	20 dB
G_{R_r}	RF receive antenna gain	20 dB
λ_r	RF links wavelength	0.158 m

In Figure 2, the performance of both schemes, i.e., the one introduced in this paper, labeled as "Proposed Scheme", and the one that always selects the highest SNR, labeled as "Maximum SNR", is evaluated using the criteria of OP (using (25)), the NLE (using (28)), and the SP (using (29)). The performance of these criteria is evaluated as a function of switching threshold $\gamma_{\rm th}$, assuming that $\frac{\gamma_T}{\bar{\gamma}_k} = -10$ dB. It is shown that as $\gamma_{\rm th}$ increases, the OP performance of the proposed scheme approaches the one of maximum SNR. What is very important to note is that the proposed scheme offers a considerable improvement in overhead estimation criteria that have been examined in this paper, namely, the NLE and PS. For example, for $\gamma_{\rm th} = 5$ dB, the OP is equal for both schemes; SP is 10–14% lower for the proposed scheme, while the NLE is more than 70% lower. Therefore, based on the results of this figure, it can be concluded that in the proposed scheme, an excellent compromise between performance improvement and overhead reduction can be achieved by setting $\gamma_{\rm th} = \gamma_T$. It is noted that by setting $\gamma_{\rm th} = \gamma_T$ in (17), it can be easily mathematically proved that the CDF expressions of the two policies coincide. Nevertheless, for the numerical results that follow, equal values for these two thresholds have been considered.

In Figure 3, an effort to depict the impact of the wind velocity w on the OP has been made. More specifically, the OP is plotted as a function of the average SNR (assuming $\bar{\gamma}_1 = \bar{\gamma}_2$). In this figure, it is shown that the OP improves as the wind velocity increases, with the highest improvement being noticed when w decreases from 51 m/s to 31 m/s. In the same figure and using the corresponding high SNR expression for the CDF, based on (26) and (27), excellent tightness between the exact and the asymptotic results is proved. In Figure 4, the impact of the elevation angle θ on the OP of the proposed scheme has been evaluated. More specifically, the OP is plotted as a function of the average SNR for various values of θ. It is shown that the performance improves as θ decreases. Moreover, an excellent tightness is also observed between the exact and the asymptotic results. In both Figures 3 and 4, it can be seen that the corresponding performance of the scheme that always selects the link that offers the maximum received SNR is always equal to the one of the proposed scheme, verifying the discussion that followed Figure 2.

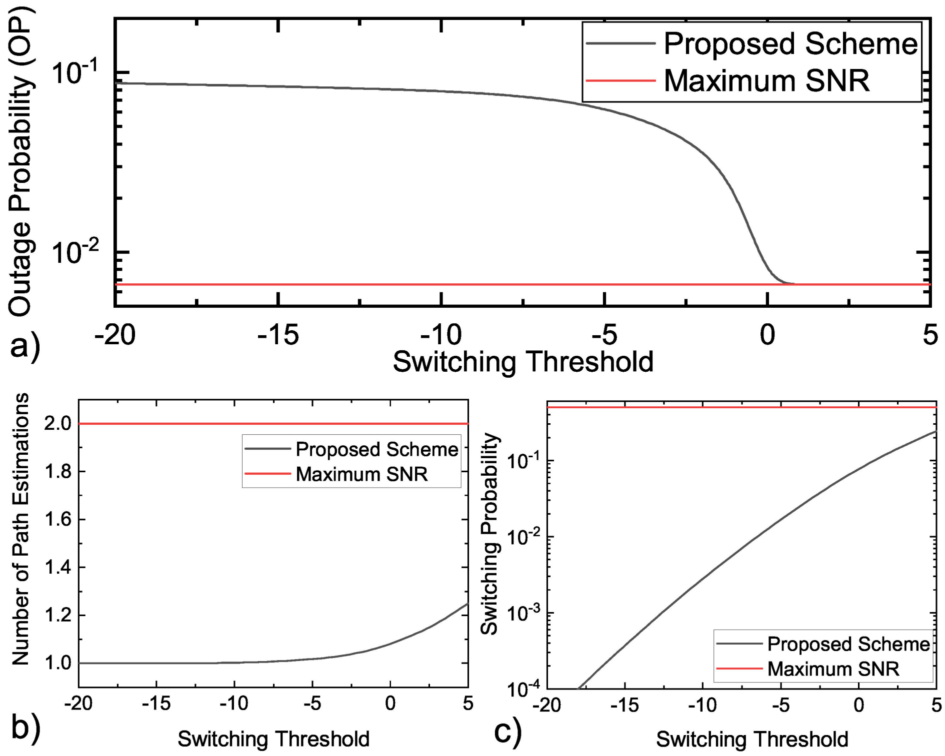

Figure 2. Proposed scheme's OP performance and complexity analysis. (**a**) Outage probability vs. switching threshold, (**b**) number of path estimations vs. switching threshold, (**c**) switching probability vs. switching threshold.

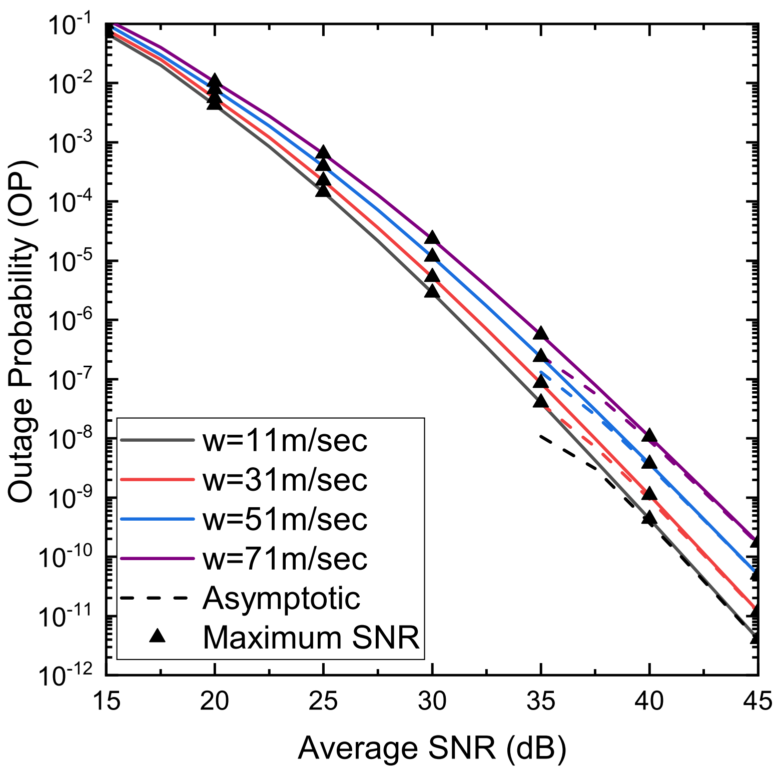

Figure 3. OP vs. average SNR for different wind velocities. The performance improves as the wind velocity decreases.

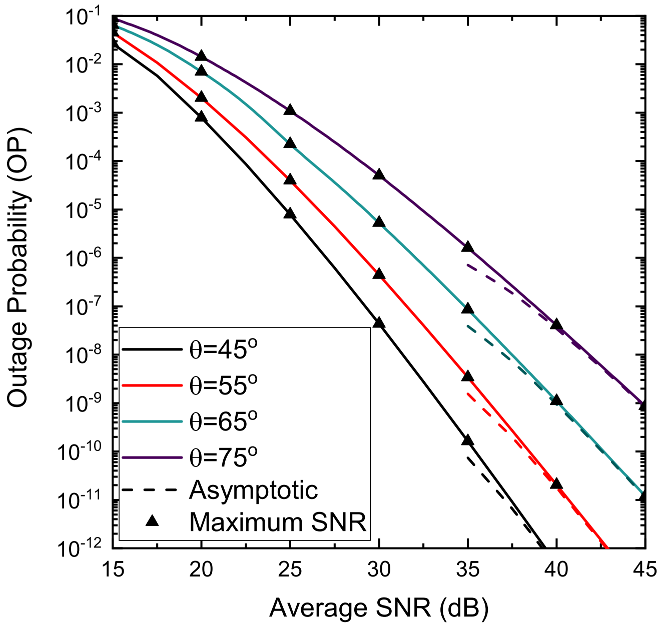

Figure 4. OP vs. average SNR for different elevation angles. The performance improves as θ decreases.

Finally, in Figure 5, the impact of small- and large-scale fading, which are controlled by parameters m, α, respectively, on the OP and SP has been evaluated. In these figures, the important difference that exists between the two limiting scenarios, i.e., the one with light fading/shadowing conditions ($m = 3, \alpha = 1$) and the one with severe fading/shadowing ($m = 1, \alpha = 3$), is shown. For the other scenarios under investigation, it seems that when light fading and severe shadowing exists, i.e., $m = 3, \alpha = 1$, the performance is better for lower values of the average SNR, as compared to the reverse scenario. As far as the SP is concerned, it is depicted that for all scenarios investigated, except the one with good fading/shadowing conditions, as the average SNR increases the performances become equal.

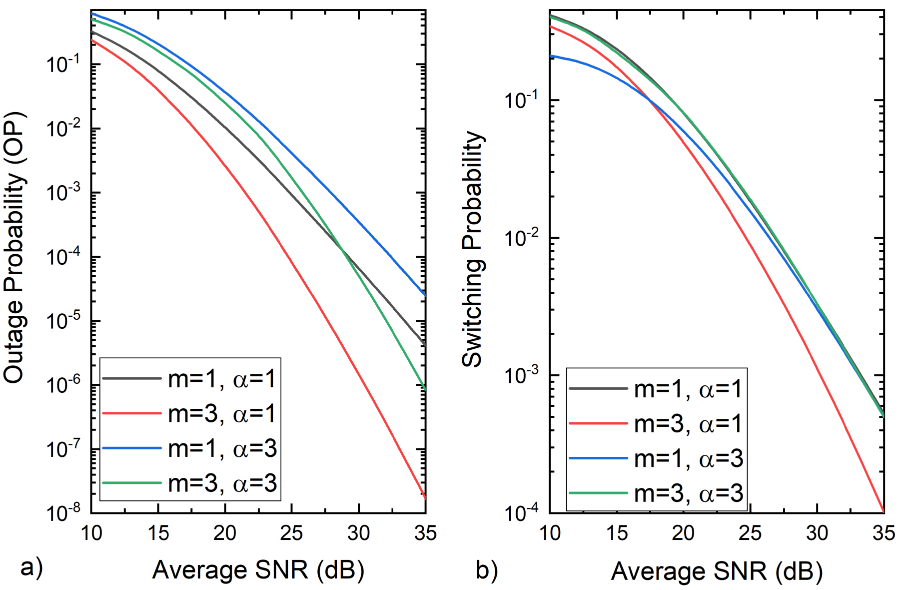

Figure 5. Performance of the proposed scheme for different propagation conditions for the RF link: (**a**) Outage probability vs. average SNR, and (**b**) switching probability vs. the average SNR.

6. Conclusions

In this paper, a new channel selection policy is employed in hybrid FSO/RF space–air–ground integrated networks. This policy can dynamically improve the system's performance or reduce the overhead signaling according to the network operator requirements. To this aim, a stochastic analysis has been performed to investigate the performance of the proposed scheme in terms of the end-to-end outage probability. Moreover, the signaling overhead has been evaluated using the criteria of switching probability and average number of link selections. It has been shown that the proposed scheme offers similar OP performance to another benchmark (whose performance was also evaluated), however with reduced overhead. As a future step, it is planned to investigate the impact of time correlated fading and outdated channel state information on the proposed system's performance.

Author Contributions: Conceptualization, P.S.B. and H.E.N.; methodology, P.S.B.; software, P.S.B.; validation, P.S.B., H.E.N., A.K. and L.Y.; writing—original draft preparation, P.S.B.; writing—review and editing, P.S.B., H.E.N., A.K. and L.Y.; visualization, P.S.B.; supervision, H.E.N. All authors have read and agreed to the published version of the manuscript.

Funding: This research received no external funding.

Data Availability Statement: Data are contained within the article.

Conflicts of Interest: The authors declare no conflicts of interest.

Abbreviations

The following abbreviations are used in this manuscript:

AWGN	Additive White Gaussian Noise
CDF	Cumulative Distribution Function
DF	Decode-and-Forward
FSO	Free Space Optical
HAPS	High-Altitude Platform Station
LAP	Low-Altitude Platform
LEO	Low Earth Orbit
NLE	Number of Link Estimation
OP	Outage Probability
PDF	Probability Density Function
RF	Radio Frequency
RIS	Reconfigurable Intelligent Surface
SAGIN	Satellite Aerial Ground Integrated Networks
SNR	Signal-to-Noise Ratio
SP	Switching Probability
UAV	Unmanned Aerial Vehicles

References

1. Liu, J.; Shi, Y.; Fadlullah, Z.M.; Kato, N. Space-air-ground integrated network: A survey. *IEEE Commun. Surv. Tutor.* **2018**, *20*, 2714–2741. [CrossRef]
2. Guo, H.; Li, J.; Liu, J.; Tian, N.; Kato, N. A survey on space-air-ground-sea integrated network security in 6G. *IEEE Commun. Surv. Tutor.* **2022**, *24*, 53–87. [CrossRef]
3. Shang, B.; Yi, Y.; Liu, L. Computing over space-air-ground integrated networks: Challenges and opportunities. *IEEE Netw.* **2021**, *35*, 302–309. [CrossRef]
4. Ye, J.; Dang, S.; Shihada, B.; Alouini, M.S. Space-air-ground integrated networks: Outage performance analysis. *IEEE Trans. Wirel. Commun.* **2020**, *19*, 7897–7912. [CrossRef]
5. Niu, Z.; Shen, X.S.; Zhang, Q.; Tang, Y. Space-air-ground integrated vehicular network for connected and automated vehicles: Challenges and solutions. *Intell. Converg. Netw.* **2020**, *1*, 142–169. [CrossRef]
6. Chowdhury, M.Z.; Hasan, M.K.; Shahjalal, M.; Hossan, M.T.; Jang, Y.M. Optical Wireless Hybrid Networks: Trends, Opportunities, Challenges, and Research Directions. *IEEE Commun. Surv. Tutor.* **2020**, *22*, 930–966. [CrossRef]

7. Anandkumar, D.; Sangeetha, R. A survey on performance enhancement in free space optical communication system through channel models and modulation techniques. *Opt. Quantum Electron.* **2021**, *53*, 5. [CrossRef]
8. Nadeem, F.; Kvicera, V.; Awan, M.S.; Leitgeb, E.; Muhammad, S.S.; Kandus, G. Weather effects on hybrid FSO/RF communication link. *IEEE J. Sel. Areas Commun.* **2009**, *27*, 1687–1697. [CrossRef]
9. Barrios, R.; Dios, F. Exponentiated Weibull distribution family under aperture averaging for Gaussian beam waves. *Opt. Express* **2012**, *20*, 13055–13064. [CrossRef] [PubMed]
10. Usman, M.; Yang, H.C.; Alouini, M.S. Practical switching-based hybrid FSO/RF transmission and its performance analysis. *IEEE Photonics J.* **2014**, *6*, 1–13. [CrossRef]
11. Kurt, G.K.; Khoshkholgh, M.G.; Alfattani, S.; Ibrahim, A.; Darwish, T.S.; Alam, M.S.; Yanikomeroglu, H.; Yongacoglu, A. A vision and framework for the high altitude platform station (HAPS) networks of the future. *IEEE Commun. Surv. Tutor.* **2021**, *23*, 729–779. [CrossRef]
12. Jia, Z.; Sheng, M.; Li, J.; Han, Z. Toward data collection and transmission in 6G space–air–ground integrated networks: Cooperative HAP and LEO satellite schemes. *IEEE Internet Things J.* **2021**, *9*, 10516–10528. [CrossRef]
13. Liu, X.; Lin, M.; Zhu, W.P.; Wang, J.Y.; Upadhyay, P.K. Outage performance for mixed FSO-RF transmission in satellite-aerial-terrestrial networks. *IEEE Photon. Technol. Lett.* **2020**, *32*, 1349–1352. [CrossRef]
14. Kong, H.; Lin, M.; Zhu, W.P.; Amindavar, H.; Alouini, M.S. Multiuser Scheduling for Asymmetric FSO/RF Links in Satellite-UAV-Terrestrial Networks. *IEEE Wirel. Commun. Lett.* **2020**, *9*, 1235–1239. [CrossRef]
15. Yang, L.; Guo, W.; Ansari, I.S. Mixed dual-hop FSO-RF communication systems through reconfigurable intelligent surface. *IEEE Commun. Lett.* **2020**, *24*, 1558–1562. [CrossRef]
16. Lei, X.; Yang, L.; Zhang, J.; Li, G.; Chen, J. LAP-Based FSO-RF Cooperative NOMA Systems. In Proceedings of the 2020 IEEE 92nd Vehicular Technology Conference (VTC2020-Fall), Victoria, BC, Canada, 18 November–16 December 2020; pp. 1–5. [CrossRef]
17. Swaminathan, R.; Sharma, S.; Vishwakarma, N.; Madhukumar, A. HAPS-based relaying for integrated space–air–ground networks with hybrid FSO/RF communication: A performance analysis. *IEEE Trans. Aerosp. Electron.* **2021**, *57*, 1581–1599.
18. Yahia, O.B.; Erdogan, E.; Kurt, G.K.; Altunbas, I.; Yanikomeroglu, H. HAPS selection for hybrid RF/FSO satellite networks. *IEEE Trans. Aerosp. Electron.* **2022**, *58*, 2855–2867. [CrossRef]
19. Yahia, O.B.; Erdogan, E.; Kurt, G.K. HAPS-assisted hybrid RF-FSO multicast communications: Error and outage analysis. *IEEE Trans. Aerosp. Electron.* **2023**, *59*, 140–152. [CrossRef]
20. Samy, R.; Yang, H.C.; Rakia, T.; Alouini, M.S. Hybrid SAG-FSO/SH-FSO/RF transmission for next-generation satellite communication systems. *IEEE Trans. Veh. Technol.* **2023**, *72*, 14255–14267. [CrossRef]
21. Li, X.; Li, Y.; Song, X.; Shao, L.; Li, H. RIS Assisted UAV for Weather-Dependent Satellite Terrestrial Integrated Network with Hybrid FSO/RF Systems. *IEEE Photonics J.* **2023**, *15*, 7304217. [CrossRef]
22. Michailidis, E.T.; Bithas, P.S.; Nomikos, N.; Vouyioukas, D.; Kanatas, A.G. Outage probability analysis in multi-user FSO/RF and UAV-enabled MIMO communication networks. *Phys. Commun.* **2021**, *49*, 101475. [CrossRef]
23. Sharif, S.; Zeadally, S.; Ejaz, W. Space-aerial-ground-sea integrated networks: Resource optimization and challenges in 6G. *J. Netw. Comput. Appl.* **2023**, *215*, 103647. [CrossRef]
24. Viswanath, A.; Jain, V.K.; Kar, S. Analysis of earth-to-satellite free-space optical link performance in the presence of turbulence, beam-wander induced pointing error and weather conditions for different intensity modulation schemes. *IET Commun.* **2015**, *9*, 2253–2258. [CrossRef]
25. Sharma, S.; Madhukumar, A.; Ramabadran, S. Performance of dual-hop hybrid FSO/RF system with pointing errors optimization. In Proceedings of the IEEE 91st Vehicular Technology Conference, Virtual Event, 25–28 May 2020; pp. 1–5.
26. Kaushal, H.; Kaddoum, G. Optical communication in space: Challenges and mitigation techniques. *IEEE Commun. Surv. Tutor.* **2016**, *19*, 57–96. [CrossRef]
27. Gradshteyn, I.S.; Ryzhik, I.M. *Table of Integrals, Series, and Products*, 6th ed.; Academic Press: New York, NY, USA, 2000.
28. Viswanath, A.; Gopal, P.; Jain, V.K.; Kar, S. Performance enhancement by aperture averaging in terrestrial and satellite free space optical links. *IET Optoelectron.* **2016**, *10*, 111–117. [CrossRef]
29. Bithas, P.S.; Nikolaidis, V.; Kanatas, A.G.; Karagiannidis, G.K. UAV-to-Ground communications: Channel modeling and UAV selection. *IEEE Trans. Commun.* **2020**, *68*, 5135–5144. [CrossRef]
30. Bithas, P.S.; Rontogiannis, A.A.; Karagiannidis, G.K. An Improved Threshold-Based Channel Selection Scheme for Wireless Communication Systems. *IEEE Trans. Wirel. Commun.* **2016**, *15*, 1531–1546. [CrossRef]
31. Bertsekas, D.; Tsitsiklis, J.N. *Introduction to Probability*; Athena Scientific: Nashua, NH, USA, 2008; Volume 1.
32. Abramowitz, M.; Stegun, I.A. *Handbook of Mathematical Functions: With Formulas, Graphs, and Mathematical Tables*; Courier Corporation: Chelmsford, MA, USA, 1964; Volume 55.
33. The Wolfram Functions Site. 2024. Available online: https://functions.wolfram.com/ (accessed on 7 January 2024).